

The Development of Advanced Electrode Materials for Environmentally Sustainable Mg-O₂/CO₂ Fuel Batteries

Po-Yuan Chang¹, Pin Ko², Po-Jen Tseng³, Jia-Yaw Chang^{1*}

¹ Department of Chemical Engineering, National Taiwan University of Science and Technology

² Department of Chemical and Materials Engineering, Chung Cheng Institute of Technology, National Defense University

³ Taiwan Semiconductor Manufacturing Co., Ltd.

(*Corresponding Author: jychang@mail.ntust.edu.tw)

ABSTRACT

The term "carbon capture and storage" (CCS) pertains to the technological process of capturing and subsequently storing carbon dioxide (CO₂). Our research team is currently engaged in the development of a "metal-air fuel cell" with the objective of effectively capturing CO₂ from the atmosphere, regardless of its concentration. In this study, we present the utilization of liquidambar Formosana fruit (LFF) as a potential gas diffusion electrode (GDE) for battery applications. Our findings reveal that this natural GDE exhibits a much higher battery discharge specific capacity density of 1441.4 wh/kg compared to conventional electrodes. Furthermore, the evaluated battery life using the LFF-based GDE is seen to be 7.77 times longer than that of alkaline AA batteries. In addition, the utilization of the advanced adsorption material known as active charcoal resorcinol-formaldehyde (ACRF) has demonstrated a notable enhancement in the adsorption capability of CO₂, reaching a value of 4.52 mmol/g at standard conditions of 1.00 bar and 298.15 K. This innovative technology is designed to effectively purify the air by simultaneously absorbing oxygen and CO₂, while converting them into direct current (DC) power and valuable chemical compounds. Not only is it capable of capturing CO₂, but it also possesses the ability to store and subsequently utilize it. The development of a cost-effective and highly efficient optimal CCS technology solution is a promising pathway towards achieving economic, environmental, and sustainability objectives.

Keywords: Renewable Energy Resources, Carbon Capture, Carbon Storage, Negative Emissions System, Fuel Cells, Bioenergy Utilization

NOMENCLATURE

Abbreviations

CCS	Carbon Capture and Storage
LFF	Liquidambar Formosana Fruit
GDE	Gas Diffusion Electrode
ACRF	Active Charcoal Resorcinol-Formaldehyde
RF	Resorcinol-Formaldehyde
IL	Ionic Liquid

1. INTRODUCTION

Given that forests, soils, and seas have the capacity to serve as natural carbon sinks for carbon dioxide (CO₂) [1], it is important to note that these sinks have experienced a gradual saturation in recent times. Consequently, to mitigate the release of CO₂ into the atmosphere resulting from the present emissions of fossil fuel waste gases, it is imperative to prioritize the absorption of CO₂. CCS has gained widespread recognition as a viable and efficient approach for reducing carbon emissions [2-4]. The recently invented "Metal-CO₂ Fuel Cells" primarily produce electrical energy through the oxidation-reduction interaction between active metals and oxygen (O₂) and CO₂, resulting in metal carbonates or bicarbonates forming. The product C_n (n ≥ 2) possesses the capability to undergo reproduction processes that facilitate the concentration of CO₂ into various chemical compounds. This phenomenon can be likened to converting CO₂ into electricity and valuable chemicals, while also enabling the capture of CO₂ [5-8]. Metal-CO₂ fuel cells often utilize metals with negative standard reduction potentials, such

as lithium, sodium, Mg, and aluminum, at the anode. This selection is made to achieve a higher operating voltage and energy density [9, 10]. Metallic CO₂ batteries that

utilization of CO₂. The primary focus of the research was developing an efficient adsorption material, as illustrated in Figure 1. The carbonized phenolic resin exhibits a

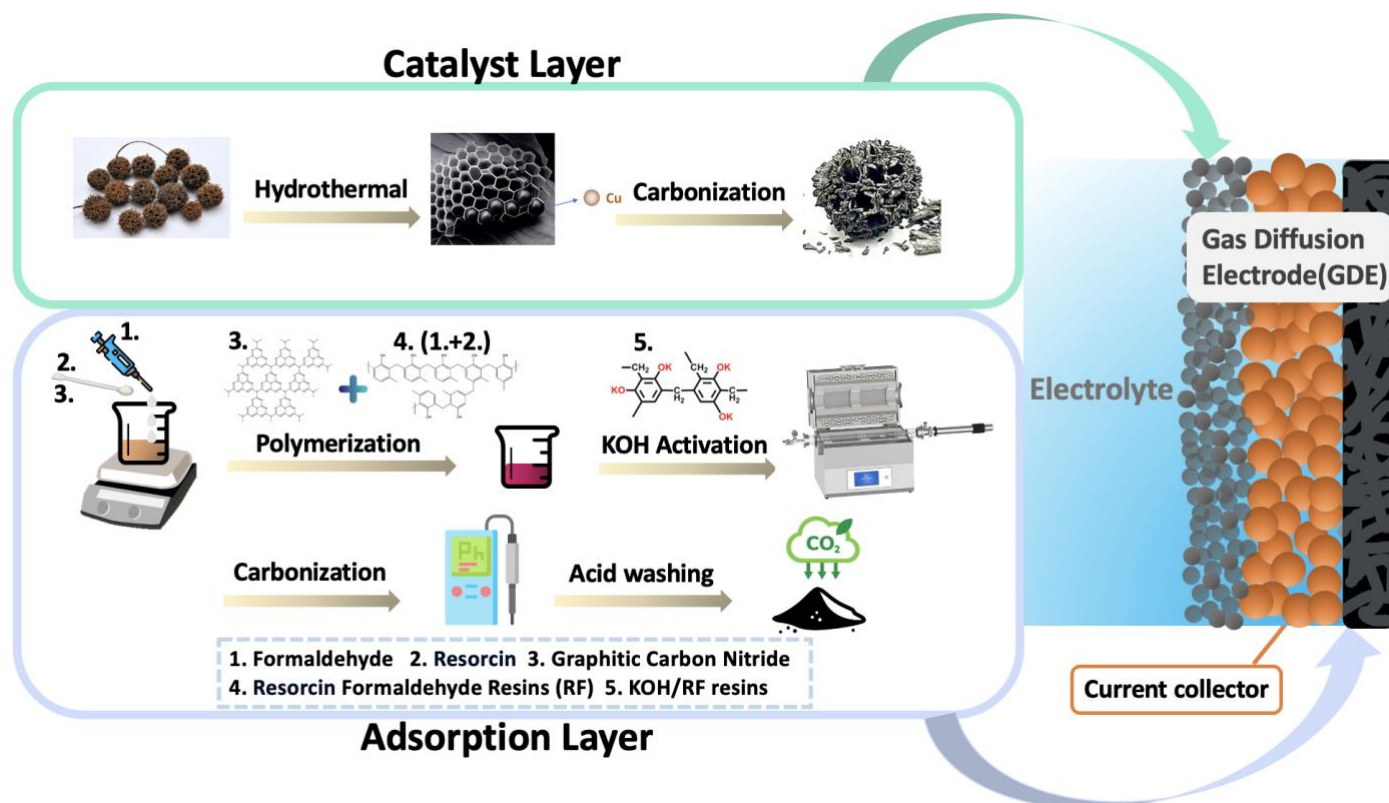


Fig. 1. LFF and gC₃N₄-ACRF schematic diagram

utilize organic electrolytes can directly transform CO₂ feedstock into solid products, such as Li₂CO₃, Na₂CO₃, or Al₂(CO₃)₂. These solid products accumulate on the surface of the electrode, leading to a decrease in the electrochemical activity of the electrode. Consequently, this reduction in electrochemical activity results in a limited discharge capacity [11–14]. The advantageous safety profile of Mg and its minimal environmental toxicity compensates for its lower energy density compared to lithium and sodium, rendering it a desirable choice as an anode metal in Mg-CO₂ batteries [15]. In aluminum-CO₂ batteries utilizing pure CO₂ as the cathode active material, the limited reactivity of aluminum necessitates adding a certain quantity of O₂ as an auxiliary gas to enhance the electrochemical performance significantly. The utilization of ionic liquid (IL) as the electrolyte in the aluminum-CO₂/O₂ battery results in a discharge voltage of around 1.4 V, with the primary discharge product being Al₂(C₂O₄)₃ [16]. In this study, a novel approach was devised to optimize the

significant presence of well-developed and tightly dispersed ultra-micropores [17], resulting in an exceptional ability to capture CO₂. The molar concentration of the substance is 4.52 millimoles per gram at a pressure of 1.00 bar and a temperature of 298.15 Kelvin. Furthermore, our research endeavors involve developing electrocatalytic materials with enhanced efficiency in conjunction with renewable energy sources. Our research aims to mitigate greenhouse gas emissions and foster sustainable resource utilization [18, 19]. This study investigates the integration of adsorbents and catalysts to develop a primary battery. Specifically, the objective is to prevent the release of captured CO₂ during the charging process. The results indicate that the Mg-based battery system exhibits a consistent discharge performance of 15.39 hours at room temperature under constant power discharge conditions of 400 mW. The research topic is illustrated in Figure 2.

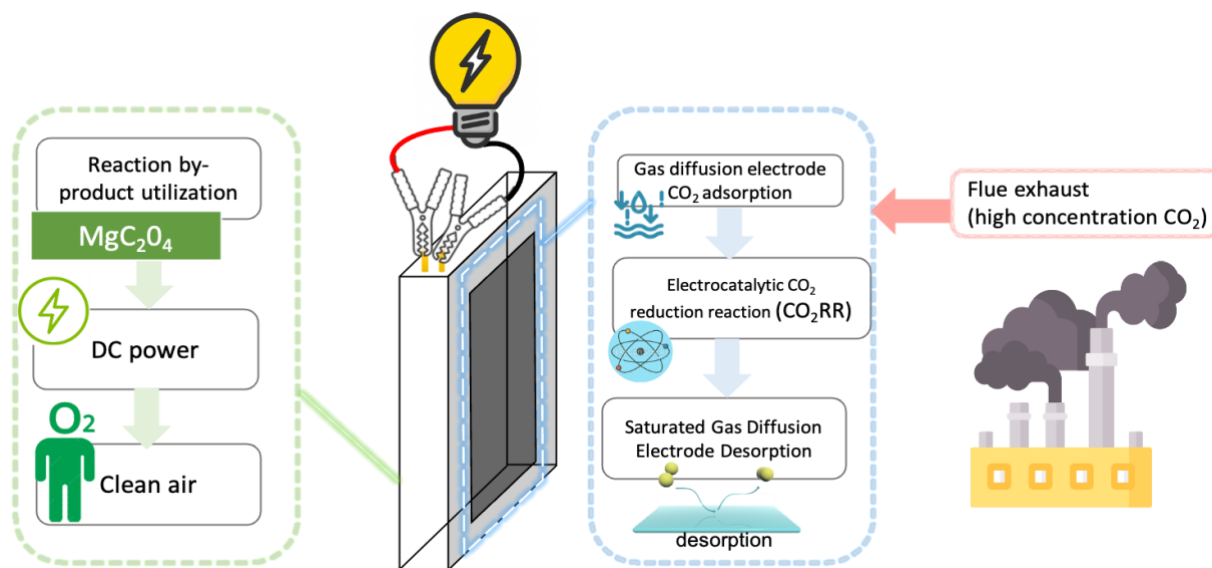


Fig. 2. A schematic representation of the operational cycle of a Mg-O₂/CO₂ fuel battery.

2. EXPERIMENTAL SECTION

2.1 Chemical and reagents

Formaldehyde (HCHO) was bought from Thermal Scientific. Resorcinol was procured from Emperor Chemical Co., LTD. Potassium hydroxide (KOH) was purchased from Honeywell. Hydrochloric acid (HCl) was bought from FLUKA-Honyewell. Copper Acetate (Cu(CH₃COO)₂) was procured from Acros Organics. All purchased chemicals were used directly without any further processing unless otherwise stated.

2.2 Synthesis of biomass activated carbon

The LFF were immersed in 100 mL of deionized water for 6 hours at a temperature of 25 °C. The initial mass of the LFF was 10 g. The capsules that had been saturated were subsequently extracted and subjected to additional purification steps, including acetone and ethanol solutions to eliminate any contaminants. The experimental procedure involves placing the saturated copper acetate solution and pre-treated seeds into a Teflon tank, which is subsequently sealed within an autoclave to conduct a hydrothermal reaction. The reaction is carried out under certain conditions, namely a temperature of 160 degrees Celsius for a duration of 12 hours. Subsequently, the carbonization and calcination process are executed under the conditions of 800°C for 1 hour, with a heating rate of 10°C per minute, producing biomass-activated carbon.

2.3 g-C₃N₄ composite porous resin-based activated carbon

During the production of RF resin spheres, varying quantities of g-C₃N₄ were included. Acquire the RF Resin Ball. 10 ml, 3M Potassium hydroxide (KOH) was employed as an activating agent to initiate the activation process, which was subsequently followed by carbonization at a temperature of 800 °C for a duration of 1 hour, with a heating rate of 10 °C per minute. Following the process of carbonization, the resulting product was then cooled to the surrounding ambient temperature. It was then subjected to a thorough washing procedure, including using a hydrochloric acid solution with a concentration of 1 M and deionized water. This washing process aimed to effectively eliminate any remaining KOH traces from the sample. Subsequently, the acquired samples underwent a drying process beyond 10 hours. The as-prepared sample is denoted as g-C₃N₄-ACRF(X), where X represents the mass of g-C₃N₄ added. The values of X used in this study are 0.1, 0.25, 0.75, 1, and 1.5 g, respectively. To facilitate comparison, samples that did not have g-C₃N₄ added were generated and labeled as ACRF.

2.4 Material Characterization

The micromorphology analysis of the copper-doped bioenergy carbon materials and g-C₃N₄ composite porous resin-based activated carbons was conducted using a field-emission scanning electron microscope (JEOL, JSM 7900F) operating at 15 kV. The CO₂ adsorption capacity of the as-synthesized samples were determined using a high-pressure gas adsorption meter (MICROTRAC, BELSORP HP). The tests involved the adsorption of CO₂ at two different temperatures, specifically 0°C and 25°C. The pressure range explored throughout these experiments was between 0 and 1.0

bar. The surface chemical characteristics were assessed using an energy-dispersive spectrometer (Oxford Instruments, Ultim Max 100).

2.5 Gas Diffusion Electrode (GDE) Preparation

The electrochemical analysis GDE was created by applying a coating consisting of 70 wt% active material (comprised of biogenic activated carbon doped with Cu, with commercial activated carbon serving as the control) and 30 wt% polytetrafluoroethylene (PTFE) binder. The preparation of the composite slurry composition was conducted. The application of the material onto the copper mesh is achieved by the doctor blade method, wherein the copper mesh serves as the collection grid. Subsequently, the composite coating was dried at 70 °C for 12 hours. The GDE that was manufactured underwent a cutting process to get dimensions of 1 × 1 cm² to facilitate electrochemical measurements.

2.6 Electrochemical testing of half-cell configurations

In the experimental setup, a graphite carbon rod was employed as the counter electrode, while an Ag/AgCl electrode was utilized as the reference electrode, thereby establishing a three-electrode system. The electrolyte used in the studies is a 1M NaCl solution, and an electrochemical impedance analyzer (CH Instrument, CHI 700E) is employed for measurements in all half-cell configurations.

2.7 Full battery measurement

The charge and discharge performance of the complete battery were evaluated using an electrochemical impedance analyzer (Admiral Instrument, Sqiudstat Plus). The battery configuration primarily employs a Mg metal sheet as the anode, with the cathode consisting of a GDE. The electrolyte utilized in this configuration is an aqueous solution of 3M NaCl. The density of catalyst loading was measured to be 15 mg cm⁻², and the area of catalyst loading normalized the current density.

3. RESULTS AND DISCUSSION

The recently created "Mg-O₂/CO₂ fuel cell" represents an environmentally friendly energy storage device designed for the purpose of carbon dioxide extraction. The schematic representation of the battery's structure is illustrated in Figure 3. During the process of operation, the primary method of electricity generation is the oxidation-reduction reaction between the active metal Mg and CO₂. The fundamental composition of a battery consists of three main components: the anode, cathode, and intermediary electrolyte. During the

process of discharge, the anode, composed of Mg metal, undergoes oxidation, releasing electrons. The flow of electrons occurs within the circuit, leading them to the cathode, a porous carbon electrode. The electrons combine with oxygen, water, and CO₂ at this location to generate oxalate ions. Carbon, in and of itself, does not engage in reactions and furnish active sites for reactions, thereby resulting in the absence of any loss. The oxalate ions will ultimately traverse the intermediary electrolyte and react with Mg²⁺ ions, forming Mg oxalate. The overarching process might be likened to an energy storage mechanism that effectively absorbs and transforms carbon dioxide into electrical energy. The following is the reaction chemical equation of Mg-O₂/CO₂ fuel cell:

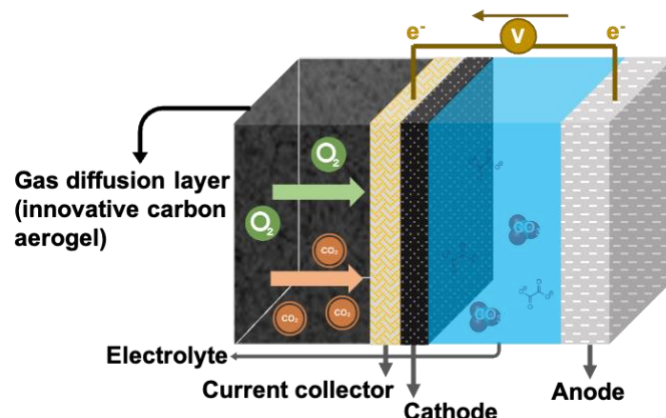
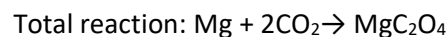
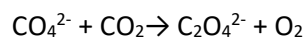
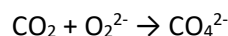
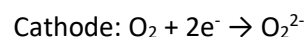
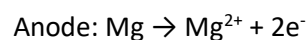


Fig. 3. Structural diagram of Mg-O₂/CO₂ fuel battery

3.1 Microscopic morphology and chemical properties of porous LFF and gC₃N₄-ACRF

The scanning electron microscopy (SEM) images depict the RF resin and the carbon substance ACRF in their original states. The presence of numerous dense and homogeneous pore structures in ACRF is evident. The size of the pores depicted in Figure 4(a), is around 50 nm, proving that these pores are primarily responsible for ACRF's notable capacity for adsorbing carbon dioxide. Furthermore, the gC₃N₄-ACRF with porous structure, was synthesized by including additional g-C₃N₄ as the nitrogen precursor for the material. The presence and prominent identification of the pore structure can be shown in Figure 4(b). The gC₃N₄-ACRF(0.25) exhibits non-

uniform pore size, characterized by the presence of mesopores and large pores. Furthermore, the pore diameter indicates a decreasing trend from the outer to the inner regions. It can be deduced that this particular structure can assimilate higher amounts of CO₂ effectively and facilitates efficient gas diffusion. The surface morphology of LFF, as depicted in Figure 4(c), exhibits a porous structure and a much smoother surface. The gC₃N₄-ACRF material has the capability to adsorb CO₂, which may then be desorbed and transferred to the LFF material. This process facilitates CO₂ reduction and enhances electrocatalytic functions.

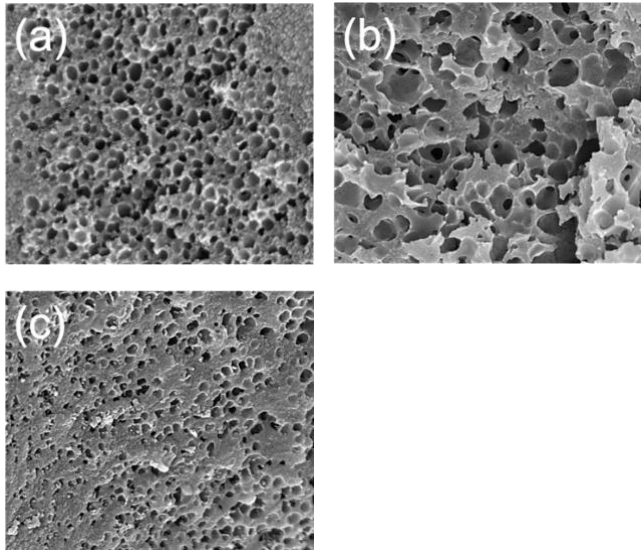


Fig. 4. SEM images of (a) ACRF, (b) gC₃N₄-ACRF(0.25), (c) LFF

In examining Energy-dispersive spectroscopy (EDS), Figure 5(a) illustrates the elemental composition of ACRF, indicating that the carbon component constitutes the entirety of the background value, excluding hydrogen and oxygen. In Figure 5(b), the observation of the wavefront of nitrogen allows for the determination that gC₃N₄-ACRF(0.25) is a composite activated carbon material with a nitrogen component. Similarly, it is evident from Figure 5(c) that LFF exhibits a distinct presence of copper, indicating its amalgamation with biomass-activated carbon. The detection results of EDS mapping Figure 6 are consistent with the anticipated outcomes. Both gC₃N₄-ACRF(0.25) and LFF exhibit high carbon signal density with a uniformly scattered nitrogen signal. Ultimately, the observed signal of LFF is comparatively diminished, so substantiating the efficacy of copper ion doping by the hydrothermal technique.

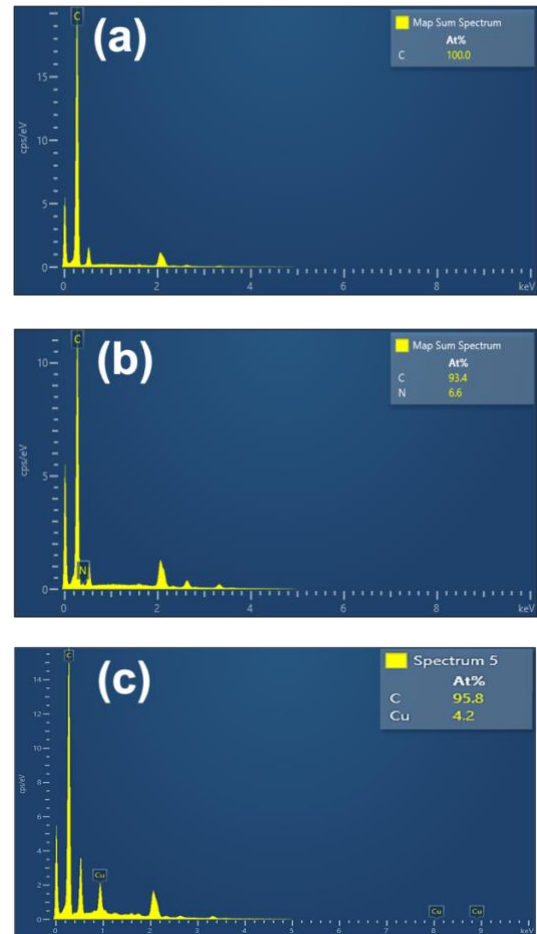


Fig. 5. EDS of (a) ACRF, (b) gC₃N₄-ACRF(0.25), (c) LFF

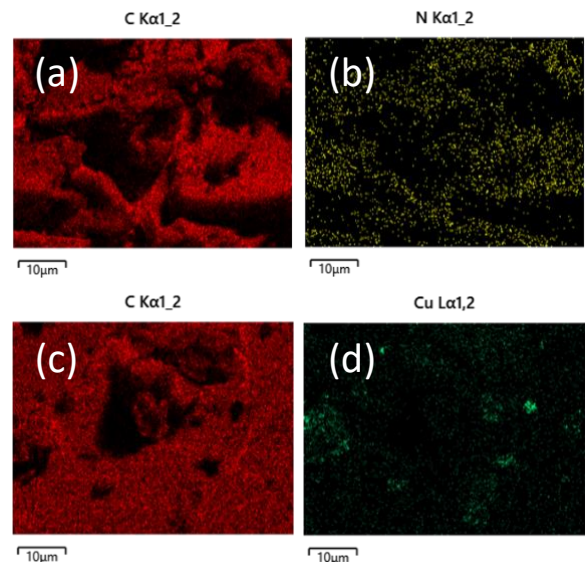


Fig. 6. EDS mapping images of (a-b) gC₃N₄-ACRF(0.25), (c-d) LFF

3.2 CO₂ capture performance of porous resin-based activated carbon

In a general sense, the ability of CO₂ to store under typical pressure conditions is mainly influenced by micropores with diameters less than 1 nm. Conversely, the storage capacity of CO₂ at high-pressure conditions is

intricately linked to both micropores and mesopores. The significant factors under consideration are the ultra-microporosity and low total pore volume, less than $0.9 \text{ cm}^3/\text{g}$. Consequently, we investigated the adsorption capability of CO_2 on the $\text{gC}_3\text{N}_4\text{-ACRF}$ sample under ambient pressure conditions. According to the data presented in Figure 7., it was observed that the adsorbent developed in this study had a remarkable capacity for capturing CO_2 . Among the samples tested, $\text{gC}_3\text{N}_4\text{-ACRF}(0.25)$ demonstrated the most significant CO_2 absorption levels, with 302.21 mg/g at 0°C , 1bar and 198.81 mg/g at 25°C , 1 bar, respectively. This can be ascribed to the fact that it possesses the highest micropore volume. The observed value of 198.81 mg/g exceeds that of other phenolic resin-based porous carbon compounds when subjected to the same conditions. In Figure 7., it is noteworthy to mention that the CO_2 adsorption capacity of $\text{gC}_3\text{N}_4\text{-ACRF}(0.25)$ surpasses that of previously documented adsorbent materials, including CO_2 -activated carbon spheres [21], nitrogen-rich microporous carbon spheres [22], porous carbon nitride spheres, KOH activated carbon spheres, and hollow carbon spheres [23]. The exceptional CO_2 adsorption capability of $\text{gC}_3\text{N}_4\text{-ACRF}$ can be primarily due to its extensively produced ultra-micropores characterized by a consistent pore size.

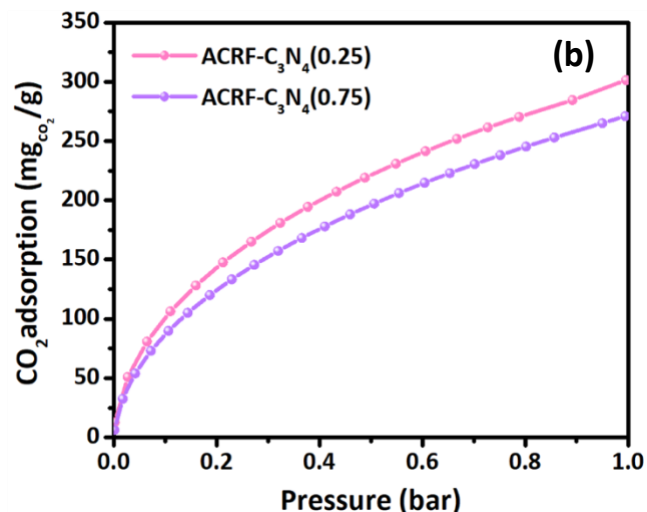
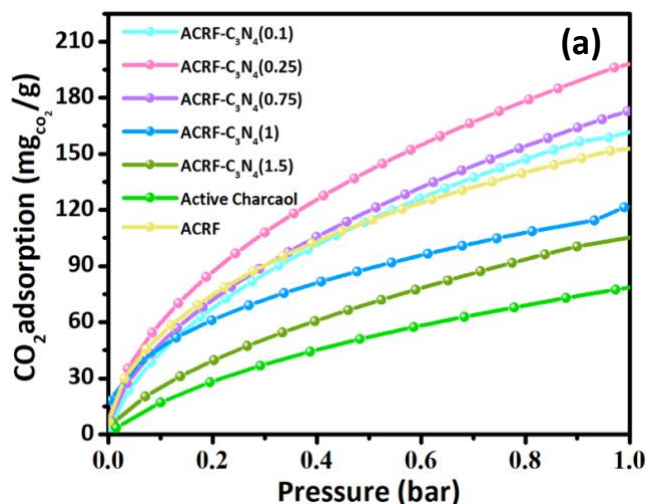


Fig.7. CO_2 adsorption measurements (a) at 25°C , 1 bar (b) at 0°C , 1 bar

3.3 Electrochemical performance of biomass activated carbon

Electrochemical impedance spectroscopy (EIS) was subsequently employed to investigate the electron/ion transport mechanism of the LFF electrode. The EIS spectrum was obtained and analyzed by employing an analogous circuit, which is illustrated in Figure 8. In the low-frequency range, it has been shown that only activated carbons that are commercially available exhibit mass transport segments, so indicating that. Biomass-derived activated carbons have enhanced mass transfer rates and typically lack a mass transfer segment that can be attributed to the presence of a highly porous structure or favorable surface diffusion properties. Consequently, a reaction that limits the overall rate does not impede the mass transfer process. The primary determinant is that there will not be a discernible mass transfer segment depicted on the EIS. The symbol (R_s) is used to denote the combined resistance arising from the intrinsic resistance of the electrode material, the ionic resistance of the electrolyte, and the contact resistance between the electrode and the current collector. On the other hand, the symbol (R_{ct}) is employed to represent the resistance associated with charge transfer. Based on the provided Figure 8., the R_s value remains relatively consistent. This suggests that the observed resistance is likely attributable to the electrolyte under the same experimental conditions. Additionally, the R_{ct} value for LFF is comparatively lower than the other samples. The presence of doped nano-copper ion LFF indicates the existence of a diverse microstructure. The porous structure of the pores facilitates rapid ion/charge transfer in electrochemical processes and reduces the distance over which ions must travel, hence improving the electrocatalytic performance.



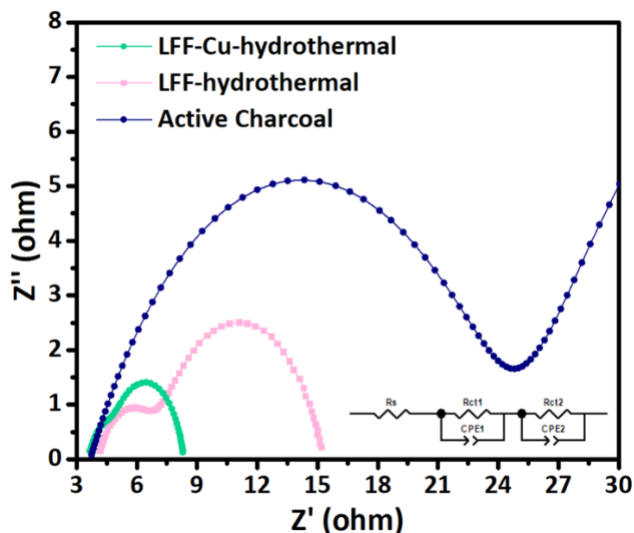


Fig. 8. Nyquist plot of different activated carbon

Table 1. Impedance results of different activated carbons

	Rs	Rct1	Rct2
LFF-Cu-hydrothermal	3.49	1.28	3.45
LFF-hydrothermal	4.02	2.98	8.53
Active charcoal	3.73	21.01	–

3.4 Full cell performance of Mg-O₂/CO₂ fuel battery

In order to showcase the operational efficiency of the Mg-O₂/CO₂ fuel battery, electrodes consisting of a 1 mm thick Mg metal sheet and self-synthesized biomass-activated carbon were employed. The anode and cathode are designated as such, with the cathode comprising a self-constructed GDE. As depicted in Figure 9. The electrolyte remains free from any supplementary chemicals, and a pristine solution of 3M NaCl brine is employed as the electrolyte. The utilization of Mg metal as the primary material in the battery



Fig. 9 GDE image

discharge process necessitates implementing a double-cathode design (see Figure 10.) to optimize the effectiveness of the Mg metal oxidation reaction. The test item was primarily chosen for steady power discharge at a rate of 200 mW. The commercially available alkaline AA battery was used as the partnering group. The load voltage of the Mg-O₂/CO₂ system is within the range of 1-1.1 V, exhibiting superior stability when compared to alkaline AA batteries. The endurance performance of the Mg-O₂/CO₂ fuel cell is 1.47 times greater than that of the alkaline AA battery. The quantity of Mg flakes consumed during the entire discharge process amounts to 2.12 grams. The electric capacity is determined to be 1357.13 mAh/g, although the precise energy density remains unspecified. The energy density is measured to be 1441.38 Wh/kg. The discharge performance of Mg-O₂/CO₂ fuel battery is exceptional and noteworthy. The termination of the discharge response occurred at 15.39 hours. It is evident that the Mg sheet has been completely depleted, and an observation was made regarding the penetration of the Mg sheet into the reaction zone, resulting in battery polarization.

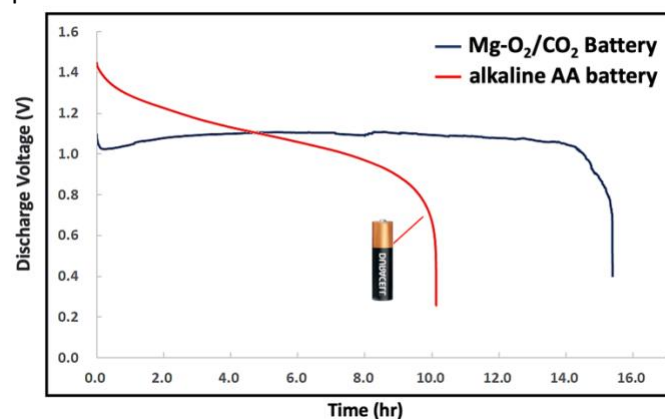


Fig. 10 Capacitance test of Mg-O₂/CO₂ fuel battery and alkaline AA battery at 200 mW constant power discharge

4. CONCLUSION

To realize the technical idea of CCS, we have successfully concluded the development of a Mg-O₂/CO₂ battery. This encompasses the creation of the cathode adsorption layer, the catalytic layer, and the design and structure of the battery as a whole. We aim to establish a fully functional metal-air fuel cell for efficient gas exchange. In this study, the natural fruit is modified to produce activated carbon, which is subsequently utilized in biomass energy as a GDE component. The specific capacity density of battery discharge is significantly larger than conventional electrodes, achieving a 1441.4 wh/kg. The activated carbon material gC₃N₄-ACRF, which has been created with high efficiency, exhibits a remarkable adsorption capacity for carbon dioxide,

measuring 4.52 mmol/g under conditions of 1.00 bar and 298.15 K. This characteristic makes it very suitable for carbon capture. During the conclusive examination, the Mg-O₂/CO₂ fuel battery demonstrates a consistent discharge duration of 15.39 hours under a constant power output. Furthermore, its operational lifespan is 7.77 times longer than that of the alkaline AA battery. The potential application of the Mg-O₂/CO₂ fuel battery in electronic devices is anticipated in the future, with the aspiration of its utilization as a handy power production mechanism.

ACKNOWLEDGEMENT

The authors want to acknowledge financial support from National Science and Technology Council of the Republic of China (Contract No. NSTC 112-2113-M-011-002).

REFERENCE

[1] Pan, Y., Birdsey, R. A., Fang, J., Houghton, R., Kauppi, P. E., Kurz, W. A., & Hayes, D. (2011). A large and persistent carbon sink in the world's forests. *Science*, 333(6045), 988-993.

[2] Boot-Handford, M. E., Abanades, J. C., Anthony, E. J., Blunt, M. J., Brandani, S., Mac Dowell, N., & Fennell, P. S. (2014). Carbon capture and storage update. *Energy & Environmental Science*, 7(1), 130-189.

[3] Bui, M., Adjiman, C. S., Bardow, A., Anthony, E. J., Boston, A., Brown, S., & Mac Dowell, N. (2018). Carbon capture and storage (CCS): the way forward. *Energy & Environmental Science*, 11(5), 1062-1176.

[4] Gibbins, J., & Chalmers, H. (2008). Carbon capture and storage. *Energy policy*, 36(12), 4317-4322.

[5] Gao, S., Lin, Y., Jiao, X., Sun, Y., Luo, Q., Zhang, W., ... & Xie, Y. (2016). Partially oxidized atomic cobalt layers for carbon dioxide electroreduction to liquid fuel. *Nature*, 529(7584), 68-71.

[6] Rosen, B. A., Salehi-Khojin, A., Thorson, M. R., Zhu, W., Whipple, D. T., Kenis, P. J., & Masel, R. I. (2011). Ionic liquid-mediated selective conversion of CO₂ to CO at low overpotentials. *Science*, 334(6056), 643-644.

[7] Chang, S., Liang, F., Yao, Y., Ma, W., & Yang, B. (2018). Research progress of metallic carbon dioxide batteries. *Acta Chimica Sinica*, 76(7), 515.

[8] Zhang, S., Kang, P., Ubnoske, S., Brennaman, M. K., Song, N., House, R. L., & Meyer, T. J. (2014). Polyethylenimine-enhanced electrocatalytic reduction of CO₂ to formate at nitrogen-doped carbon nanomaterials. *Journal of the American Chemical Society*, 136(22), 7845-7848.

[9] Wang, F., Li, Y., Xia, X., Cai, W., Chen, Q., & Chen, M. (2021). Metal-CO₂ electrochemistry: from CO₂ recycling

to energy storage. *Advanced Energy Materials*, 11(25), 2100667.

[10] Xie, Z., Zhang, X., Zhang, Z., & Zhou, Z. (2017). Metal-CO₂ batteries on the road: CO₂ from contamination gas to energy source. *Advanced Materials*, 29(15), 1605891.

[11] Jin, Y., Hu, C., Dai, Q., Xiao, Y., Lin, Y., Connell, J. W., & Dai, L. (2018). High-performance Li-CO₂ batteries based on metal-free carbon quantum dot/holey-graphene composite catalysts. *Advanced Functional Materials*, 28(47), 1804630.

[12] Pipes, R., He, J., Bhargava, A., & Manthiram, A. (2019). Efficient Li-CO₂ batteries with molybdenum disulfide nanosheets on carbon nanotubes as a catalyst. *ACS Applied Energy Materials*, 2(12), 8685-8694.

[13] Xu, S., Das, S. K., & Archer, L. A. (2013). The Li-CO₂ battery: a novel method for CO₂ capture and utilization. *RSC advances*, 3(18), 6656-6660.

[14] Qie, L., Lin, Y., Connell, J. W., Xu, J., & Dai, L. (2017). Highly rechargeable lithium-CO₂ batteries with a boron- and nitrogen-codoped holey-graphene cathode. *Angewandte Chemie International Edition*, 56(24), 6970-6974.

[15] Das, S. K., Xu, S., & Archer, L. A. (2013). Carbon dioxide assist for non-aqueous sodium-oxygen batteries. *Electrochemistry Communications*, 27, 59-62.

[16] Zhao, Q., Zachman, M. J., Al Sadat, W. I., Zheng, J., Kourkoutis, L. F., & Archer, L. (2018). Solid electrolyte interphases for high-energy aqueous aluminum electrochemical cells. *Science advances*, 4(11), eaau8131.

[17] Wang, X., Zhou, J., Xing, W., Liu, B., Zhang, J., Lin, H., & Zhuo, S. (2017). Resorcinol-formaldehyde resin-based porous carbon spheres with high CO₂ capture capacities. *Journal of energy chemistry*, 26(5), 1007-1013.

[18] Kalyani, P., & Anitha, A. (2013). Biomass carbon & its prospects in electrochemical energy systems. *International Journal of Hydrogen Energy*, 38(10), 4034-4045.

[19] Karimi, M., Shirzad, M., Silva, J. A., & Rodrigues, A. E. (2022). Biomass/Biochar carbon materials for CO₂ capture and sequestration by cyclic adsorption processes: A review and prospects for future directions. *Journal of CO₂ Utilization*, 57, 101890.

[20] Li, J., Cheng, T., Ma, X., Wu, H., & Yang, L. (2023). A hydrophobic and hierarchical porous resin-based activated carbon modified by g-C₃N₄ for toluene capture from humid conditions. *Separation and Purification Technology*, 308, 122902.

[21] Sevilla, M., Parra, J. B., & Fuertes, A. B. (2013). Assessment of the role of micropore size and N-doping in

CO₂ capture by porous carbons. *ACS applied materials & interfaces*, 5(13), 6360-6368.

[22] Liu, L., Xie, Z. H., Deng, Q. F., Hou, X. X., & Yuan, Z. Y. (2017). One-pot carbonization enrichment of nitrogen in microporous carbon spheres for efficient CO₂ capture. *Journal of Materials Chemistry A*, 5(1), 418-425.

[23] Feng, S., Li, W., Shi, Q., Li, Y., Chen, J., Ling, Y., ... & Zhao, D. (2014). Synthesis of nitrogen-doped hollow carbon nanospheres for CO₂ capture. *Chemical Communications*, 50(3), 329-331.